Silver niobate doped lead-free perovskite KNN ceramics

IOP Conf. Series: Materials Science and Engineering **848** (2020) 012072 doi:10.1088/1757-899X/848/1/012072

Silver niobate doped lead-free perovskite KNN ceramics

E D Politova[1,2], G M Kaleva[1,2], N V Golubko[1], A V Mosunov[1], N V Sadovskaya[3], D A Kiselev[4,5], A M Kislyuk[4], T S Ilina[4], S Yu Stefanovich[1,6]

[1]L.Ya.Karpov Institute of Physical Chemistry; Vorontsovo pole, 10, Moscow 105064 Russia,
[2]Semenov Institute of Chemical Physics, Russian Academy of Sciences, Kosugina, 4, Moscow 119991 Russia,
[3]FSRC «Crystallography and Photonics» RAS, Leninskiy Prospekt 59, 119333, Moscow, Russia
[4]National University of Science and Technology "MISiS", Leninskii pr. 4, Moscow 119049 Russia,
[5]Fryazino branch of the Kotel'nikov Institute of Radioengineering and Electronics of Russian, Academy of Sciences, Vvedensky Square 1, Fryazino, Moscow region, 141190 Russia,
[6]Lomonosov Moscow State University, Leninskie gory 1, Moscow 119992 Russia

E-mail: politova@nifhi.ru

Abstract. Influence of $AgNbO_3$ doping on structure, microstructure, dielectric, ferroelectric and local piezoelectric properties of $(K_{0.5}Na_{0.5})NbO_3$ ceramics was studied. Decreased in the unit cell parameters correlated with ionic radii changes. High effective local d_{33} piezoelectric coefficient values (800 pm/V) were observed in compositions studied.

1. Introduction

Potassium-sodium niobate $(K,Na)NbO_3$ (KNN) perovskite ceramics are intensively studied last ten years as the most promising materials for replacement the toxic lead oxide containing materials [1 - 18]. The composition $(K_{0.5}Na_{0.5})NbO_3$ is close to the MPB between two orthorhombic phases and is characterized by two phase transitions near 470 K between ferroelectric phases and at 670 K between ferroelectric and paraelectric phases [10].

It should be noted that narrow sintering temperature interval for KNN-based ceramics comprises special problem, and difficulties in preparation of stoichiometric compositions due to the presence of high volatile potassium and sodium oxides [11 - 15]. Besides, the formation of oxygen vacancies in nonstoichiometric compounds leads to an increase in ionic conductivity of the samples [16-18].

Silver niobate $AgNbO_3$-based oxides showed great potential for use in power energy storage systems due to their high energy storage density. In [19], an investigation was performed analyzing the chemical structure and physical properties of $AgNbO_3$. The results confirmed that the dielectric anomaly at ~440 K originated from a phase transition between the non-centrosymmetric weakly polar and centrosymmetric non-polar phases. The weakly polar phase exhibiting antipolar ordered behavior was proposed to be ferrielectric one responsible for the strong field-induced double-like polarization hysteresis. The dielectric relaxor behavior at ~340 K correlates with the presence of local ferroelectric-type polar domains in a weakly polar/ferrielectric phase. The observed weak remnant polarization within double-like polarization hysteresis under strong field cycles was explained as originating from the polarization contributed by the

residual strong field-induced ferroelectric phase. In this work, influence of $AgNbO_3$ additive on properties of KNN composition was studied.

2. Experimental

Ceramic samples $(1-x)(K_{0.5}Na_{0.5})NbO_3 - xAgNO_3$ with x = 0.0 - 0.10, Δx=0.02 were prepared by the sol-gel synthesis, annealed at T_1=673-773 K (4 h), T_2= 1073 K (6 h) and sintered at T_3= 1373-1393 K (2 h.

As initial reagents, tetrahydrate of sodium potassium tartrate $KNaC_4H_4O_6 \cdot 4H_2O$ ("pure"), silver nitrate $AgNO_3$ ("pure" containing 99.9 % of main substance) and niobium oxide Nb_2O_5 ("pure") were used.

Stoichiometric mixtures of salts and oxide were mixed in distilled water till their complete dissolving. Then the suspension was evaporated, annealed at 673-773 K (4 h), mixed in ethanol, pressed in tablets, annealed at 1073 K (6 h) and sintered at 1373-1393 K (2 h).

To improve sintering of ceramics the compositions were additionally modified by small amounts of overstoichiometric LiF additives (5 w. %) in order to improve the sintering of ceramics [16, 17].

Phase content and crystal structure parameters of ceramic samples prepared were characterized by the X-ray Diffraction method (DRON-3M, Cu-K_α radiation with wavelength λ=1.5405 A, in the 2 theta range of 5 – 70 degrees). Spontaneous polarization and phase transitions of the samples were studied by the Second Harmonic Generation (SHG) method (Nd:YAG laser, λ=1.064 μm in the reflection). Dielectric measurements of ceramics with fired silver electrodes were performed on heating with 10 K/min. and cooling in the temperature interval of 300 – 1000 K, and frequency range of 100 Hz – 1 MHz using Agilent 4284 A (1 V). Microstructure of the samples was examined using the Scanning Electron Microscopy (SEM) method (JEOL YSM-7401F with a JEOL JED-2300 energy dispersive X-ray spectrometer system).

Atomic Force Microscopy in Piezoresponse Force Mode (PFM) (MFP-3D, Asylum Research, USA) method with a Ti/Ir-coated conductive tip (Asyelec-02, Asylum Research, USA) with a radius of curvature ~ 28 nm was used for local piezoelectric properties measurements. The PFM out-of-plane images (mixed signal) were scanned in the PFM Dual AC Resonance Tracking (DART) mode at 1-2 V and a frequency of ~980 kHz.

Before PFM measurements, the samples were polished using polycrystalline diamond up to the root mean square roughness reached <10 nm. Effective piezoelectric coefficient d_{33} was calculated from PFM phase and PFM amplitude hysteresis loops using Igor Pro software version 6.37 (Asylum Research, USA). All measurements were repeated at least 4 times in the different locations of the same sample with strong PFM domains contrast.

3. Results and discussion

Pure ceramic samples with orthorhombic perovskite structure were prepared (Figures 1*a,b*). Increase in sintering temperature resulted in texturing of ceramics with increase in intensity of peaks at 23 grad. (Figure 1*b*).

Slight shift of the X-Ray diffraction peaks to higher angles points to a decrease in the unit cell parameters due to introduction of smaller Ag^+ cations into A-site positions of perovskite lattice (Figure 2*a*).

The SHG method measurements confirmed the polar nature of the samples prepared indicating to their ferroelectric properties (Figure 2*b*). With increasing Ag^+ content, slight increase in intensity of the SHG signal was observed at x=0.02 that pointed to an increase in spontaneous polarization of the doped samples, while further decreasing may be attributed to more intensive coloration of the doped samples.

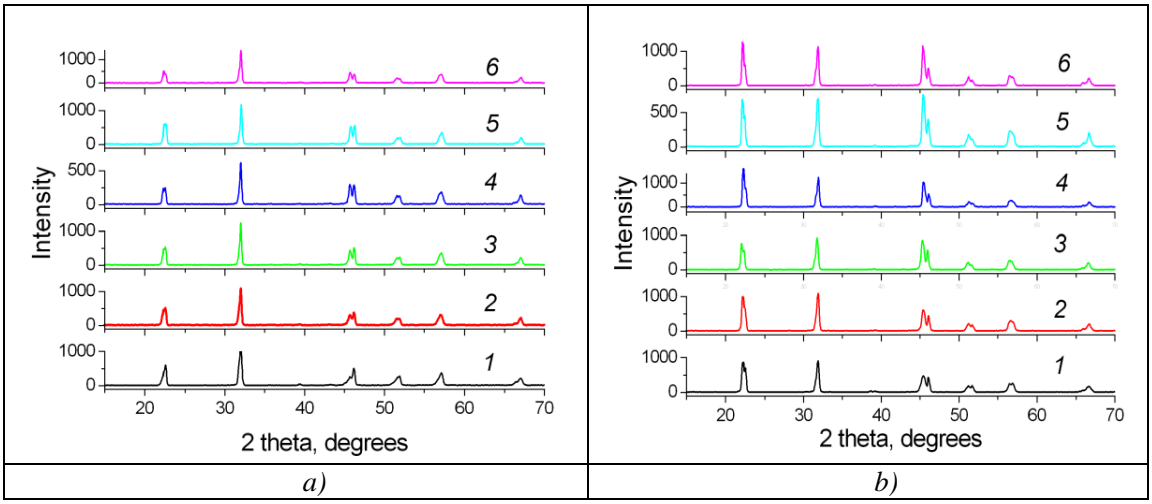

Figure 1. *a*) **-** X-Ray diffraction patterns of the samples (1-*x*)($K_{0.5}Na_{0.5}$)NbO_3 – *x*$AgNbO_3$ with *x*=0.0 (*1*), 0.02 (*2*), 0.04 (*3*), 0.06 (*4*), 0.08 (*5*), 0.10 (*6*) doped with 5 w. % LiF sintered at 1320 K (1 h). *b*) – sintered at 1320 K (5 min) → 900ºC (4 h).

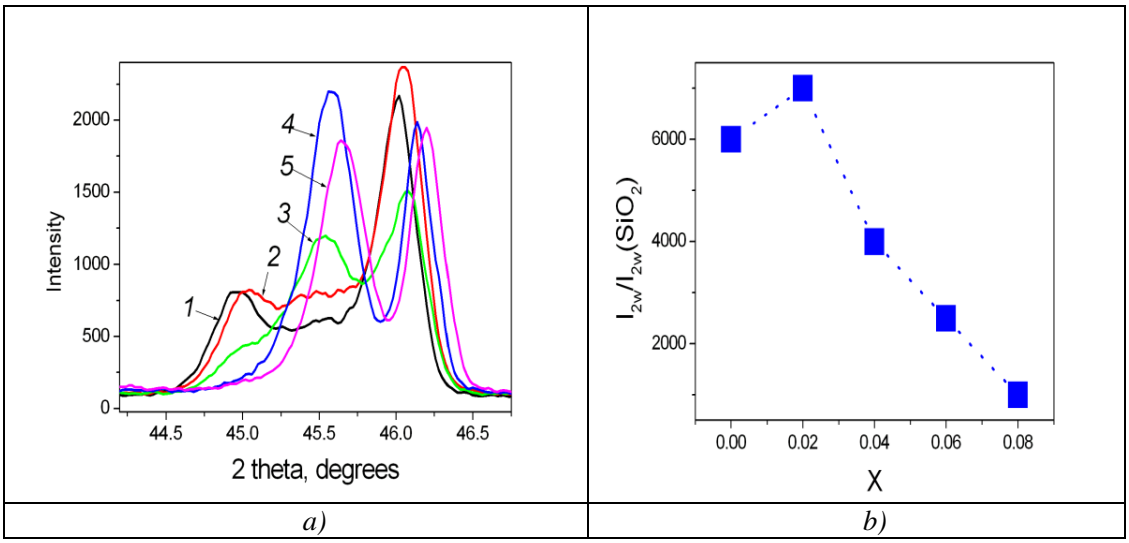

Figure 2. *a*) - Parts of the X-Ray diffraction patterns of the LiF doped samples (1-*x*)($K_{0.5}Na_{0.5}$)NbO_3 – *x*$AgNbO_3$ with *x*=0.0 (*1*), 0.02 (*2*), 0.04 (*3*), 0.06 (*4*), 0.10 (5). *b*) - Concentration dependence of the SHG signal *q* measured at the room temperature for the samples (1-*x*)($K_{0.5}Na_{0.5}$)NbO_3 – *x*$AgNO_3$ doped with 5 w. % LiF sintered at 1370 K (2 h).

Microstructure of the samples is sensitive to both substitutions and sintering conditions as well. With increasing sintering temperature enlargement of mean size of grains was observed, though mean size of grains slightly decreased with *x* increasing (Figure 3).

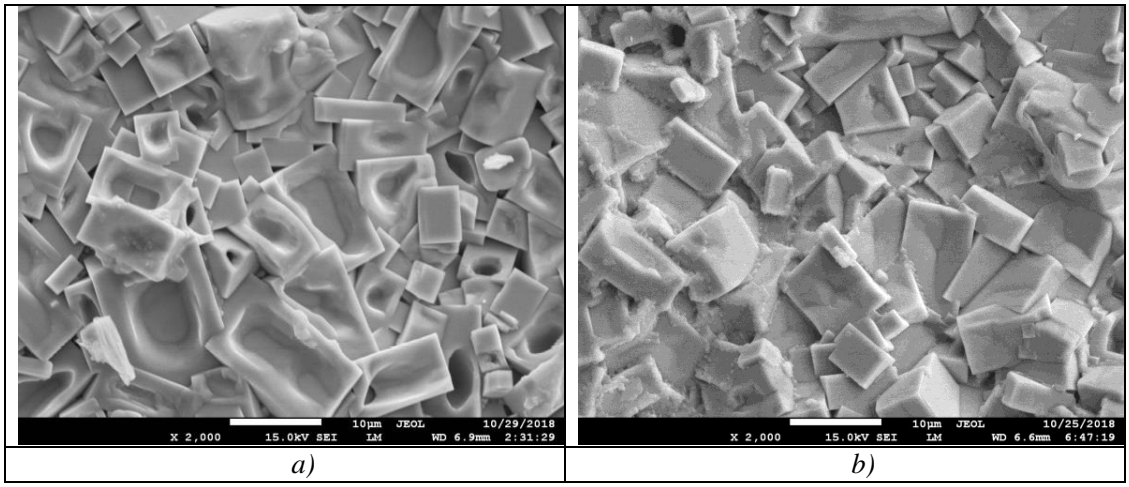

Figure 3. Microstructure of the samples with x=0.02 (*a*), 0.10 (*b*). Bars – 10 μm.

Dielectric properties of the samples were studied. Typical for the KNN-based compositions steps near ~ 350 - 400 K and maxima at ~ 600 – 700 K were revealed in the dielectric permittivity versus temperature curves (Figure 4). Slight decrease in temperature of the phase transition to paraelectric phase T_C, while an increase in the ferroelectric tetragonal to orthorhombic phase transition temperature were observed in the ceramic samples studied (Figure 5).

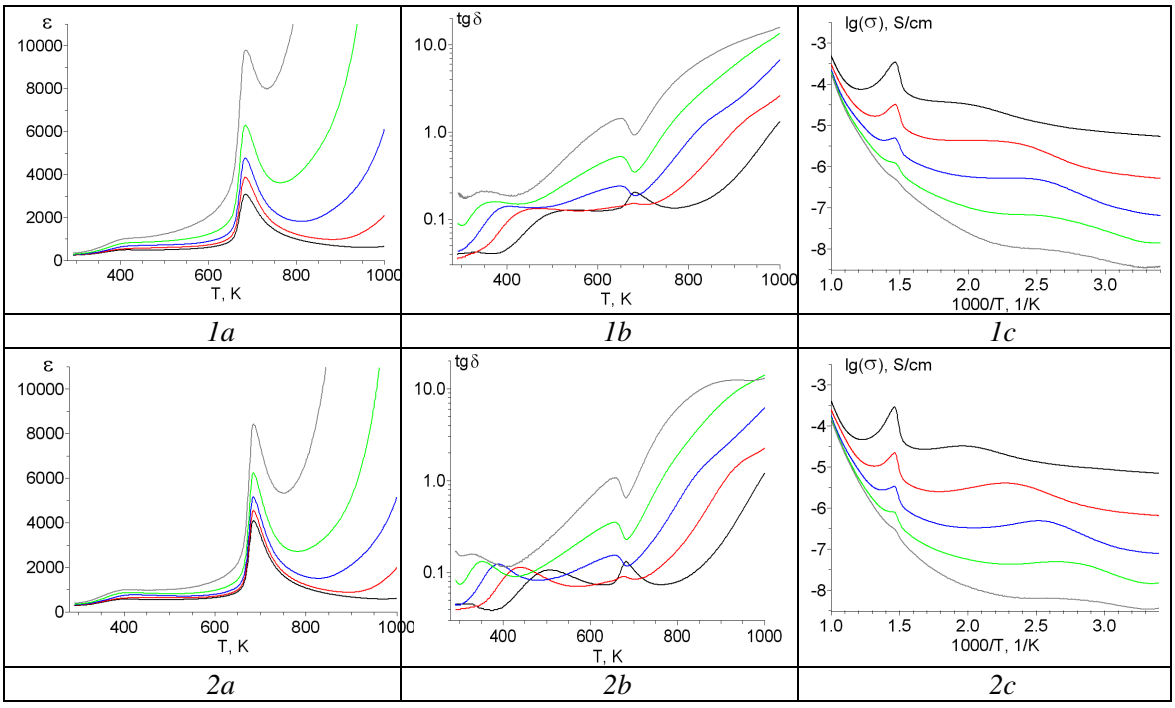

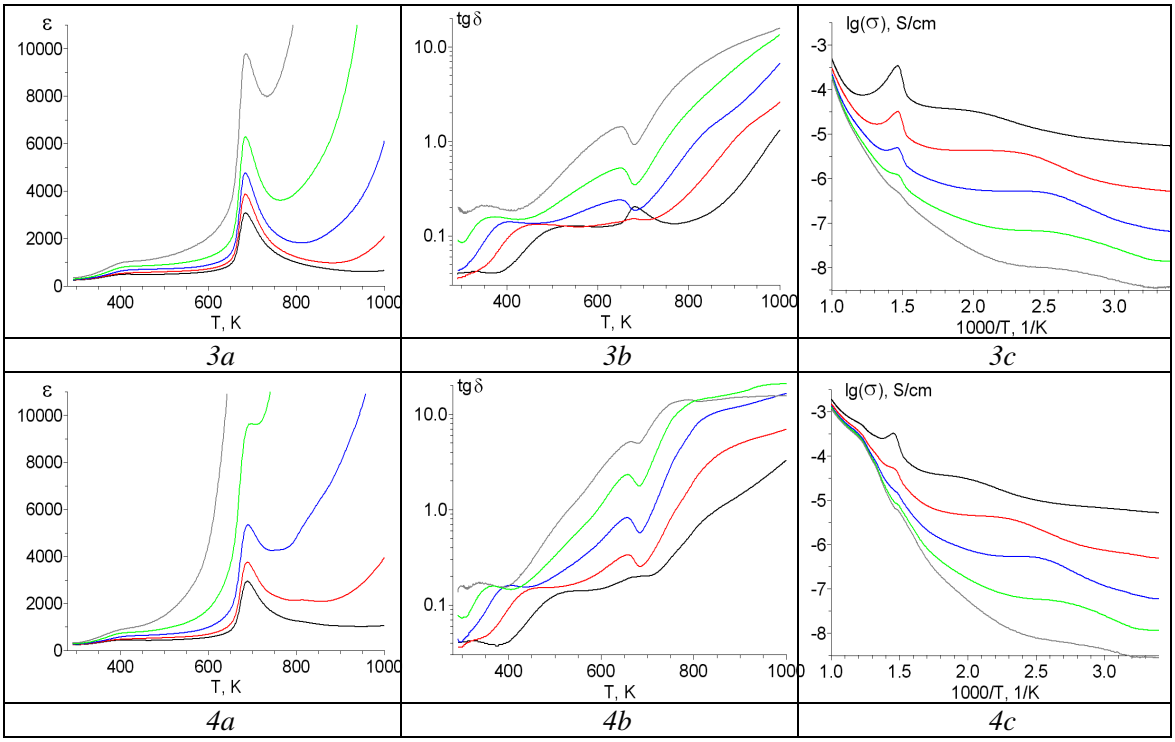

Figure 4. Temperature dependences of dielectric permittivity $\varepsilon(T)$*(a)*, dielectric loss $\tan\delta(T)$*(b)* and $\lg\sigma(1000/T)$*(c)* of the samples with x=0.0 (*1a-c*), 0.04(*2a-c*), 0.08(*3a-c*), 0.10(*4a-c*) sintered at T_3=1323 K (5 min) → T_4=1173 K (2 h) measured at frequencies f=100 Hz, 1, 10, 100 kHz, 1 MHz.

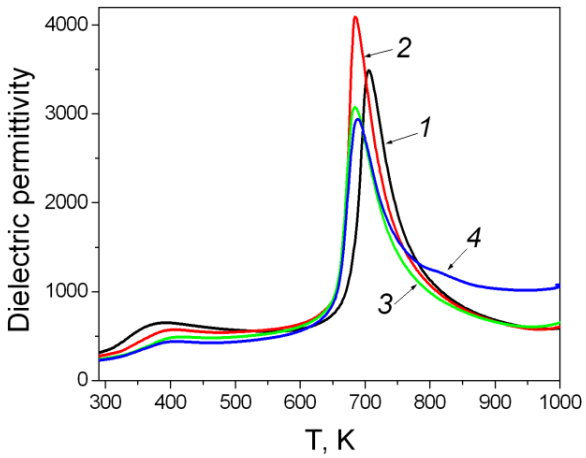

Figure 5. Temperature dependences of dielectric permittivity $\varepsilon(T)$ of the samples with x=0.0 (*1*), 0.04(*2*), 0.08(*3*), 0.10(*4*) sintered at T_3=1323 K (5 min) → T_4=1173 K (2 h) measured at frequency f = 1 MHz.

Using PFM method complex domain structure consisting of multiple domain patterns was found in investigated ceramics (Figure 6, top row). Simultaneous topography (not shown here) and out-of-plane PFM images confirmed that the imaged patterns were due to their piezoresponse [20 - 22]. To study the domain switching behavior of the Ag^{1+} ions doped KNN ceramics, 7.5×7.5 μm^2 positively polarized domains embedded in a 15×15 μm^2 equivalent negatively polarized domains were written ("box-in-box" structure). Figure 6 (middle row) presents an information of the writing voltage images, the dark and bright areas with applied –20V and +20V DC biases, respectively. Strong PFM contrast suggests complete switching process under poling for piezoelectric active grains. The domains created are stable in the time, and the PFM contrast of the written domains remained the same after 2 hours after the poling process (Figure 6, bottom row).

Local PFM hysteresis loops observed indicated ferroelectric polarization switching at nanoscale for the samples studied. An AC voltage (1-2 V) was superimposed onto a triangular square-stepping wave (f = 0.5 Hz, with writing and reading times 25 ms, and bias window up to ± 20 V) during the remnant piezoelectric hysteresis loops measurements.

Remnant hysteresis loops were received for separate grains (Figure 7*a*). All PFM hysteresis loops are asymmetric along the axis Y. According to Jesse et al., this offset may be mainly attributed to the electrostatic effect [20, 21]. Moreover, the local PFM hysteresis loops account for the polarization switching process in a nanoscale, just below the tip. Therefore, intrinsic polarization in the nanoregions may also contribute to the offset and asymmetry of the local piezoresponse hysteresis loops [22].

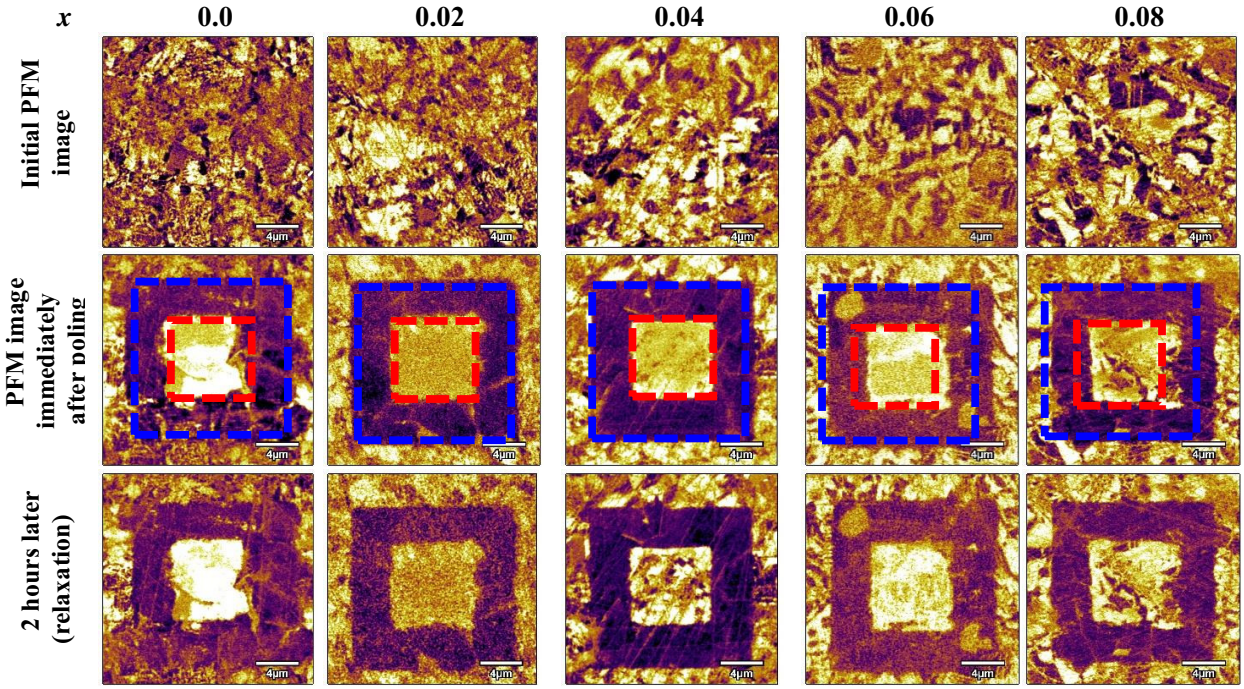

Figure 6. Initial domain structure and temporary changes of images of polarized ceramics with x=0.0, 0.02, 0.04, 0.06 and 0.08. Marked regions in the middle row present regions of 15×15 μm^2 poled with –20V DC bias and of 7.5×7.5 μm^2 poled with +20V DC bias.

The shifts along voltage axis of local PFM hysteresis loops indicate the presence of a biased-voltage due to the different contact between the top (PFM tip) moved electrode and surface of the investigated ceramic samples. The top electrode is the same (PFM tip coated Ti/Ir), so the shifts reflect the induced interface electrostatic potential step due to the built-in electric field at the interface.

Local PFM hysteresis loops revealed that remnant d_{33} piezoelectric coefficient reached the highest value of 800 pm/V for the initial KNN samples, decreased till 580 pm/V for the samples KNN-Ag with x=0.04, and then increased till 700 pm/V in the samples with x=0.08, with the saturation of loops reached at voltage value ~ 20 V (Figure 7*b*). Increase in the remnant d_{33} value at $x > 0.04$ may be explained by increasing texture of these ceramics (Figure 1*b*). The calculated value of the piezoelectric coefficient for the samples KNN-Ag is ≈ in 3-5 times larger than those previously observed for ceramic samples in the systems $(K_{0.5}Na_{0.5})NbO_3$ - $BaTiO_3$ [17] and $(K_{0.5}Na_{0.5})NbO_3$ – $Li(Nb,Mn)O_3$ [23].

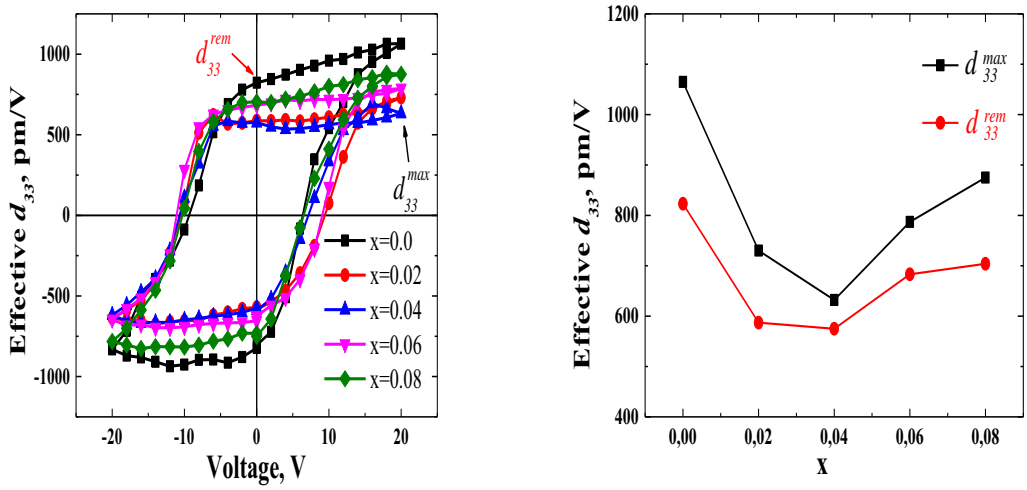

a) *b)*

Figure 7. PFM hysteresis loops (*a*), concentration dependence of effective d_{33} values of the samples with x=0.0 – 0.08 calculated from PFM hysteresis loops (*b*).

4. Conclusions

Structure, microstructure, dielectric, ferroelectric and piezoelectric properties of the $(K_{0.5}Na_{0.5})NbO_3$ ceramics doped by Ag^{1+} ions were studied. Depending on composition and sintering conditions slight changes in the unit cell volume and temperatures of phase transitions were observed. High values of the remnant d_{33} piezoelectric coefficients ~ 600 – 800 pm/V were observed for ceramics studied. This confirms their prospects for development of new efficient piezoelectric materials.

Acknowledgment

The work was supported by the Russian Foundation for Basic Research (Project 18-03-00372).). PFM studies were performed at the Center for Shared Use “Material Science and Metallurgy” at the National University of Science and Technology “MISiS” and were supported by the Ministry of High Education and Science of the Russian Federation within the framework of the state task.

References

[1] Zhang S, Xia R, and Shrout R. Lead-Free Piezoelectric Ceramics: Alternatives for PZT? 2007 *J. Electroceram.* **19**, 251-7.
[2] Takenaka T, Nagata T, and Hiruma Y. Current developments and prospective of lead-free piezoelectric ceramics. 2008 *Jpn. J. Appl. Phys.* **47**, 3787-801.
[3] Damjanovich D, Klein N, Li J and Porokhonskyy V. What can be expected from lead-free piezoelectric materials? 2010 *Funct. Mater. Lett*. **3**, 5-13.
[4] Xiao D. Progresses and further considerations on the research of perovskite lead-free piezoelectric ceramics, 2011 *J. Adv. Dielectr*. **1**, 33-40.
[5] Coondoo I, Panwar N, Kholkin A. Lead-free piezoelectrics: Current status and perspectives, 2013 *J. Adv. Dielectr*. **3**, 1330002 (22 pages).
[6] Li J, Wang K, Zhu F, Cheng L, Yao F. (K,Na)NbO_3-Based Lead-Free Piezoceramics: Fundamental Aspects, Processing Technologies, and Remaining Challenges, 2013 *J. Am. Ceram. Soc*. **96**, 3677-96.
[7] Wu J, Xiao D, Zhu J. Potassium-sodium niobate lead-free piezoelectric materials: Past, present, and future of phase boundaries, 2015 *Chem. Rev*. **115**, 2559-95.
[8] Panda P and Sahoo B. PZT to Lead-Free Piezo Ceramics, 2015 Ferroelectrics 474, 128-43.
[9] Hong C, Kim H, Choi B, Han H, Son J, Ahn C, Jo W, Lead-free piezoceramics. Where to move on? 2016 *J. Materiomics* **2**, 1-24.
[10] Dai Y, Zhang X, and Chen K, Morphotropic phase boundary and electrical properties of $K_{1-x}Na_xNbO_3$ lead-free ceramics, 2009 *Appl. Phys. Lett*. **94**, 042905.
[11] Fang J, Wang X, Zuo R, Tian Z, Zhong C, Li L. Narrow sintering temperature window for (K,Na)NbO_3-based lead-free piezoceramics caused by compositional segregation, 2011 *Phys. Status Solidi A*. **208**, 791-4.
[12] Wang K, Li J. (K,Na)NbO_3-based lead-free piezoceramics: Phase transition, sintering and property enhancement, 2012 *Adv. Ceramics* **1**, 24-37.
[13] Zuo R, Roedel J, Chen R, Li L. Sintering and electrical properties of lead-free $Na_{0.5}K_{0.5}NbO_3$ piezoelectric ceramics, 2006 *J. Am. Ceram. Soc*. **89**, 2010-5.
[14] Tellier J, Malič B, Dkhil B, Jenko D, Cilensek J, Kosec M. Crystal structure and phase transitions of sodium potassium niobate perovskites, 2009 *Solid State Sci*. **11**, 320-4.
[15] Malič B, Koruza J, Hreščak J, Bernard J, Wang K, Fisher J, Benčan A. Sintering of lead-free piezoelectric sodium potassium niobate ceramics, 2015 *Materials* **12**, 8117-46.
[16] Politova E, Kaleva G, Golubko N, Mosunov A, Akinfiev V, Stefanovich S, Fortalnova E. Influence of NaCl/LiF Additives on Structure, Microstructure and Phase Transitions of $(K_{0.5}Na_{0.5})NbO_3$ Ceramics, 2015 *Ferroelectrics* **489**, 147-55.
[17] Politova E, Golubko N, Kaleva G, Mosunov A, Sadovskaya N, Stefanovich S, Kiselev D, Kislyuk A, Panda P. Processing and characterization of lead-free ceramics on the base of sodium-potassium niobate, 2018 *J. Adv. Diel*. **8**, 1850004.
[18] Ringgaard M, and Wurlitzer T. Lead-free piezoceramics based structure, microstructure and electrical properties of alkali niobates, 2005 *J. Eur . Ceram. Soc.* **25**, 2701-6.
[19] Tian Y, Jing L, Hu Q, Jin L, Yu K, Li J, Politova E, Stefanovich S, Xu Z, Wei X. Ferroelectric Transitions in Silver Niobate Ceramics, 2019 *Journal of Materials Chemistry C* **7**, 1028-1034; DOI: 10.1039/C8TC05451G
[20] Jesse S, Baddorf A, Kalinin S. Switching spectroscopy piezoresponse force microscopy of ferroelectric materials, 2006 *Appl. Phys. Lett*. **88**, 062908.
[21] Jesse S, Kalinin S, Proksch R, Baddorf A and Rodriguez B. The band excitation method in scanning probe microscopy for rapid mapping of energy dissipation on the nanoscale, 2007

Nanotechnology **18**, 435503 (8pp) doi:10.1088/0957-4484/18/43/435503.

[22] Trivedi H, Shvartsman V, Lupascu D, Medeiros M, Pullar R, Kholkin A, Zelenovskiy P, Sosnovskikh A, Shur V. Local manifestations of a static magnetoelectric effect in nanostructured $BaTiO_3$–$BaFe_{12}O_9$ composite multiferroics, 2015 *Nanoscale* **7**, 4489-96.

[23] Politova E, Golubko N, Kaleva G, Mosunov A, Sadovskaya N, Fortalnova E, Kiselev D, Ilina T, Kislyuk A, Stefanovich S, Panda P. Ferroelectric and local piezoelectric properties of modified KNN ceramics, 2019 *Integrated Ferroelectrics* **196** (1), 52-9.